Discontinuous Galerkin methodology for Large-Eddy Simulations of wind turbine airfoils

Frere, A.; Sørensen, Niels N.; Hillewaert, K.; Winckelmans, G.

Published in:
Journal of Physics: Conference Series (Online)

Link to article, DOI:
10.1088/1742-6596/753/2/022037

Publication date:
2016

Document Version
Publisher's PDF, also known as Version of record

Discontinuous Galerkin methodology for Large-Eddy Simulations of wind turbine airfoils

2016 J. Phys.: Conf. Ser. 753 022037

(http://iopscience.iop.org/1742-6596/753/2/022037)

Discontinuous Galerkin methodology for Large-Eddy Simulations of wind turbine airfoils

A. Frère[1,2], N. N. Sørensen[3], K. Hillewaert[1], P. Chatelain[2] and G. Winckelmans[2]

[1]Cenaero, Gosselies, Belgium
[2]Université catholique de Louvain (UcL), Institute of Mechanics, Materials and Civil Engineering (iMMC), Louvain-la-Neuve, Belgium
[3]Technical University of Denmark, DTU Wind Energy, Denmark

E-mail: ariane.frere@cenaero.be

Abstract. This paper aims at evaluating the potential of the Discontinuous Galerkin (DG) methodology for Large-Eddy Simulation (LES) of wind turbine airfoils. The DG method has shown high accuracy, excellent scalability and capacity to handle unstructured meshes. It is however not used in the wind energy sector yet. The present study aims at evaluating this methodology on an application which is relevant for that sector and focuses on blade section aerodynamics characterization. To be pertinent for large wind turbines, the simulations would need to be at low Mach numbers ($M \leq 0.3$) where compressible approaches are often limited and at large Reynolds numbers ($Re \geq 10^6$) where wall-resolved LES is still unaffordable. At these high Re, a wall-modeled LES (WMLES) approach is thus required. In order to first validate the LES methodology, before the WMLES approach, this study presents airfoil flow simulations at low and high Reynolds numbers and compares the results to state-of-the-art models used in industry, namely the panel method (XFOIL with boundary layer modeling) and Reynolds Averaged Navier-Stokes (RANS). At low Reynolds number ($Re = 6 \times 10^4$), involving laminar boundary layer separation and transition in the detached shear layer, the Eppler 387 airfoil is studied at two angles of attack. The LES results agree slightly better with the experimental chordwise pressure distribution than both XFOIL and RANS results. At high Reynolds number ($Re = 1.64 \times 10^6$), the NACA4412 airfoil is studied close to stall condition. In this case, although the wall model approach used for the WMLES is very basic and not supposed to handle separation nor adverse pressure gradients, all three methods provide equivalent accuracy on averaged quantities. The present work is hence considered as a strong step forward in the use of LES at high Reynolds numbers.

1. Introduction

Wind turbine aeroelastic and wake tools use simplified aerodynamic models requiring airfoil performance data. However, these data are difficult to obtain. When reliable wind tunnel data are not available, the polar curves are obtained using codes based on panel method (e.g. XFOIL) or Computational Fluid Dynamics (CFD). CFD tools use several turbulence modeling approaches, ranging from Reynolds-Averaged Navier-Stokes (RANS) to Large-Eddy Simulation (LES), passing through hybrid approaches such as Detached-Eddy Simulation (DES) or Wall-Modeled LES (WMLES). The choice of the approach depends on the required accuracy weighted with respect to computational cost, on the flow conditions or on the information needed (average or unsteady fields). The panel (with boundary layer modeling) and RANS approaches, being

computationally much cheaper, will remain the main design tools. DES/WMLES and LES might however provide complementary results and provide more physical insights.

The Discontinuous Galerkin (DG) method has been shown to provide high order accuracy, low dissipation and low dispersion on structured and unstructured meshes, by validation on academic cases at coarse resolutions [1]. The method is highly scalable[1] and is thus a good candidate for performing LES of industrial applications [2].

As low Reynolds numbers ($Re \leq 10^5$) are only relevant for small or test scale turbines, simulations at $Re \geq 10^6$ need to be performed. These high Reynolds numbers make wall-resolved LES unaffordable and therefore impose the use of WMLES (or DES). Before validating the WMLES approach, it is crucial to validate the LES approach on airfoil flows. The DG code used in this paper has already been used to perform LES of the S826 airfoil at low Reynolds number [3]. DG LES results were very close to LES perform with a Finite Volume code (EllipSys3D) but had large discrepancies with the experiment. The discrepancies could be explained through the formation of stall cells leading to important spanwise effects and interactions with the tunnel walls, but they also motivated an evaluation of the DG LES on a low Reynolds airfoil which had more documented and consolidated experimental data. The present study is hence presenting LES of the E387 airfoil at $Re = 6\times10^4$ and WMLES of the NACA4412 airfoil at $Re = 1.64\times10^6$.

2. Methodologies

2.1. LES using Argo code

Argo, the DGM code used in this study, solves the compressible Navier-Stokes equations, using an Implicit LES (ILES) approach, in which the subgrid scale dissipation is ensured by the numerical scheme. Argo has already been successfully validated and assessed on DNS and ILES of academic benchmarks such as the DNS of transition of the Taylor-Green vortex [1] and ILES of homogeneous isotropic turbulence and channel flow [4, 5], thereby demonstrating an accuracy similar to that of dedicated academic codes. The code has already been applied to DNS of industrial benchmarks featuring transitional flow [6, 7].

At high Reynolds numbers, LES require too large computational resources due to the high resolution needed for resolving the inner part of the boundary layer, which scales as $Re^{1.9}$ [8]. At $Re = 1 \times 10^6$ for example, 99% of the mesh points are required for the inner layer, a layer which represents only $\simeq 10 - 15\%$ of the boundary layer thickness [9]. To make LES affordable at high Reynolds numbers, the inner layer needs to be modeled.

There are mainly two approaches to model the inner layer: hybrid RANS-LES, also frequently referred to as DES, and the wall-stress method or WMLES. The hybrid method (DES), introduced by Spalart *et al* [10], solves RANS equations in the inner layer and LES further away from the boundary. While this method has been applied with considerable success, for detached flows at high Reynolds numbers in particular, it is not well suited for DGM as the RANS equations are relatively challenging to solve in a DGM configuration.

The wall-stress method solves LES equations on the entire domain. At the wall, the mesh is too coarse to resolve the flow and a wall model is needed to provide the wall shear stress based on data taken at a certain distance from the wall. Considered as the most simple and robust approach from a practical point of view, the wall-stress approach was chosen for this study. Different wall models exist, with different complexities and accuracy. The simplest models are analytical relations based on the law-of-the-wall. For out of equilibrium flows, the most widely used approach is the Two-Layer Model (TLM), proposed by Balaras *et al* [11]. TLM couples LES in the free field to (a simplified versions of) the Turbulent Boundary Layer (TBL) equations near the wall.

[1] The code used in this paper provided good weak (mesh size grows with the number of processors) and strong (same mesh partitioned on ever more processors) scaling up to 1.3×10^4 cores.

In this study, a simple analytical relation is used, the Reichardt law of the wall

$$u^+ = \frac{1}{\kappa} ln\left(1 + \kappa y^+\right) + \left(C - \frac{1}{\kappa} ln\left(\kappa\right)\right)\left(1 - e^{-\frac{y^+}{11}} - \frac{y^+}{11} e^{-\frac{y^+}{3}}\right)$$

which provides the wall shear stress $\tau_w = \rho u_\tau^2$ based on the wall distance $y^+ = \frac{y\ u_\tau}{\nu}$ and the flow velocity $u^+ = \frac{u}{u_\tau}$ ($\kappa = 0.38$ and $C = 4.1$).

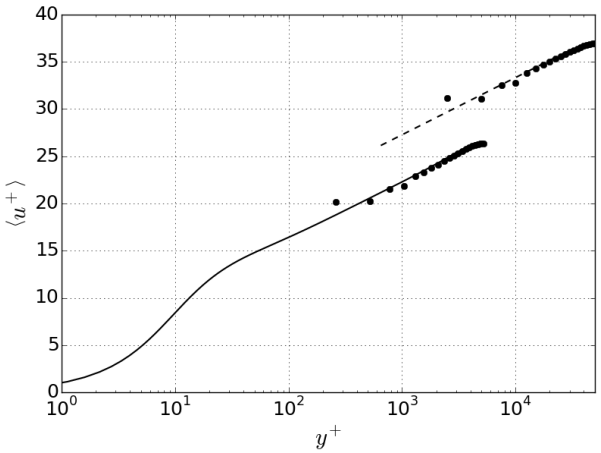

Figure 1. Wall normalized velocity profiles for channel flow at $Re_\tau = 5200$ and 5×10^5 (results translated vertically for the sake of clarity). Comparison of the WMLES results (circles) to the reference data: DNS (solid line) from [12] at $Re_\tau = 5200$ and logarithmic law of the wall (dashed line) at $Re_\tau = 5 \times 10^5$ with $\kappa = 0.38$ and $C = 4.1$.

The developed WMLES approach has been tested on a turbulent channel flow. Figure 1 shows the time-averaged velocity profiles obtained with this method on the plane channel test case for two different Reynolds numbers, $Re_\tau = 5200$ and $Re_\tau = 5 \times 10^4$. Note that the Reynolds numbers are here given in terms of the wall shear stress $Re_\tau = h\ u_\tau/\nu$; based on the bulk velocity, those would be around 2×10^5 and 3×10^6, respectively . The same mesh was used for both cases, giving a first point located at $y^+ = 250$ and $y^+ = 1800$ respectively . At both Reynolds numbers, the velocity profiles are well captured by the WMLES and they match well the DNS results [12] and the theoretical logarithmic law.

2.2. State-of-the-art methods

Both ILES and WMLES results are compared to state-of-the-art methods, namely a panel method and (U)RANS. The panel method computations are performed with XFOIL version 6.97 (with added boundary layer modeling) whereby the default settings are used except for the parameter N of the e^N transition model, parameter mimicking the environment turbulence impact on the transition and which is taken as close as possible to the wind tunnel turbulence level ($N_{crit} = 7$ for the E387 airfoil and $N_{crit} = 6$ for the NACA4412 airfoil). The RANS computations are realized using the DTU in-house incompressible finite volume RANS flow solver EllipSys2D [13, 14, 15]. In EllipSys2D, the convective terms are discretized using the QUICK scheme, as given by [16]. The simulations are carried out using Menter's $k - \omega$ SST model described in [17], while the transitional simulations are, as for XFOIL, based on the e^N model as described in [18].

2.3. Mesh configuration

The (WM)LES and (U)RANS codes have very different grid requirements. The DG code uses unstructured coarse meshes with third order polynomial interpolation within each cell, while EllipSys2D uses structured meshes and second order accurate reconstruction. Both approaches used an O-type mesh for the boundary layer and with quadrangles in the boundary layer but the (WM)LES meshes is unstructured in the far-field. The (WM)LES 3D meshes were obtained by the extrusion in the spanwise direction of the unstructured mesh. To simulate averaged spanwise homogeneity of the flow, the (WM)LES simulations impose spanwise periodicity on a span corresponding to $\approx 10\%$ of the chord.

3. LES of low Reynolds number airfoil

The Eppler 387 is a well documented airfoil which is representative of the low Reynolds flow complexity as it presents a lift hysteresis at low angles of attack and a laminar separation bubble (LSB) featuring laminar/turbulent transition in the detached shear layer. LES have been performed at $Re = 6 \times 10^4$ for two angles of attack, $\alpha = 4°$ and $8°$. Although RANS were first considered for the code comparison, URANS with $t^* = t\dot{U}/c = 5e^{-3}$ have been used here as the RANS computations could not converge without increasing unreasonably the inflow Turbulence Intensity (TI). The unsteady mode was likely needed in this case due to the burst of the laminar separation bubble.

The ILES mesh leads to computations of 2.7M dof with $\Delta y^+ \leq 1.5$ and $\Delta x^+ = \Delta z^+ \leq 20$. The RANS mesh has 384 cells in the chordwise direction and 192 cells in the normal direction placing the outer boundary 45 chords away from the airfoil, generated by the HypGrid2D code [19]. The cell spacing in the normal direction has $\Delta y/c \approx 1.5 \times 10^{-6}$ ensuring $y^+ \leq 1$.

The computational results (XFOIL, URANS and ILES) are compared to each other and to the extensive experimental data performed by McGhee *et al* [20] in the NASA Low Turbulence Pressure Tunnel. Their work provides force coefficient, chordwise pressure distribution and oil flow visualization for varying angles of attack (α), Re and inflow turbulence intensities. For the lift and drag curves, shown in Figure 2, the computations are also compared to experiments from Delft ([21]), Princeton ([22]) and Stuttgart ([23]). Please note that, as the Stuttgart original data were not available, summarized data in McGhee *et al* [20] were used.

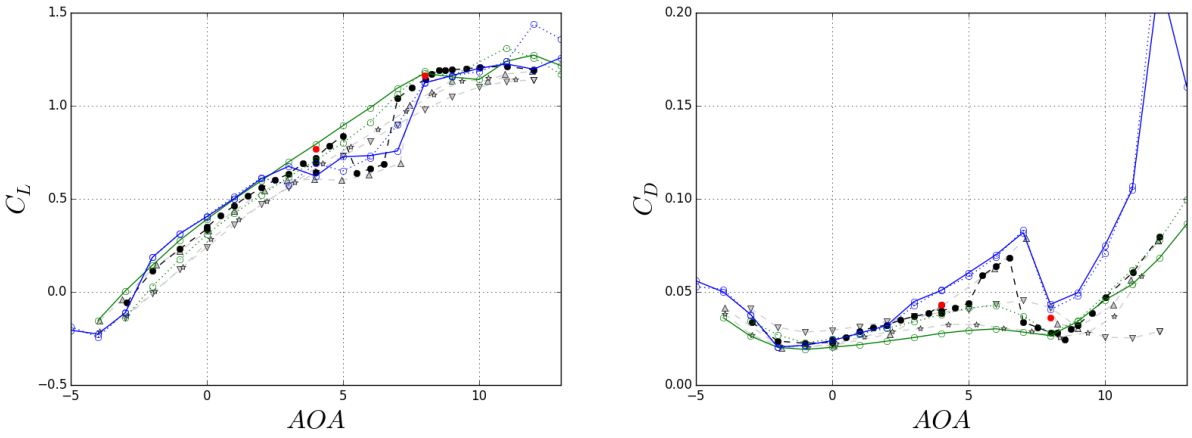

Figure 2. E387 comparison of computational lift and drag (XFOIL: green (solid for $N_{crit} = 7$,dashed for $N_{crit} = 9$), URANS: blue (solid for $N_{crit} = 7$,dashed for $N_{crit} = 9$) and ILES: red) to experiment from different wind tunnels: LTPT (black circles), Delft (up triangles), Princeton (stars), and Stuttgart (down triangles).

As XFOIL and URANS are much cheaper than LES, the full range of angles of attack are provided. The spread in the results from the different tunnels illustrate the difficulty to obtain reliable data for low Reynolds airfoils and especially for angles of attack close to the hysteresis. This is mainly due to the high sensitivity of the laminar separation bubble to the wind tunnel turbulence level. McGhee *et al* [20] observed a strong effect with respect to the TI for $\alpha \leq 7^\circ$ leading to two very different performances and flow regimes: the laminar separation with and without (turbulent/transitional) reattachment. This high sensitivity is seen in the lift curve where three different performances are observed at $\alpha = 4^\circ$. To evaluate the impact of the turbulence intensity XFOIL and URANS have been run at two different turbulence levels, with $N_{crit} = 7$ corresponding to $TI = 0.16\%$ as observed experimentally and with $N_{crit} = 9$ corresponding to $TI = 0.07\%$, i.e. almost no inflow turbulence as considered for the LES simulations. The TI effect could not be evaluated with the LES approach as its resolution would have increased drastically the computational cost. Both XFOIL and URANS show clearly the impact of the TI for $\alpha = 4^\circ$, case for which the comparison of the codes will therefore be complex. The three computational approaches provide lift coefficients very similar to those of McGhee *et al* [20] but XFOIL and LES seem to be better capturing the drag, URANS overestimating it.

The experiment showed in both cases a laminar separation followed by a laminar/turbulent transition in the shear layer and a reattachment, and that an increase in angle of attack moves the reattachment point upstream, while displacing only slightly the separation point, thereby reducing the extent of the LSB [20]. Figure 3 presents instantaneous friction and velocity fields obtained with LES; the computations can be seen to reproduce this behavior. Note that the flow remains laminar for a long distance along the airfoil and that the DG approach is hence actually performing DNS.

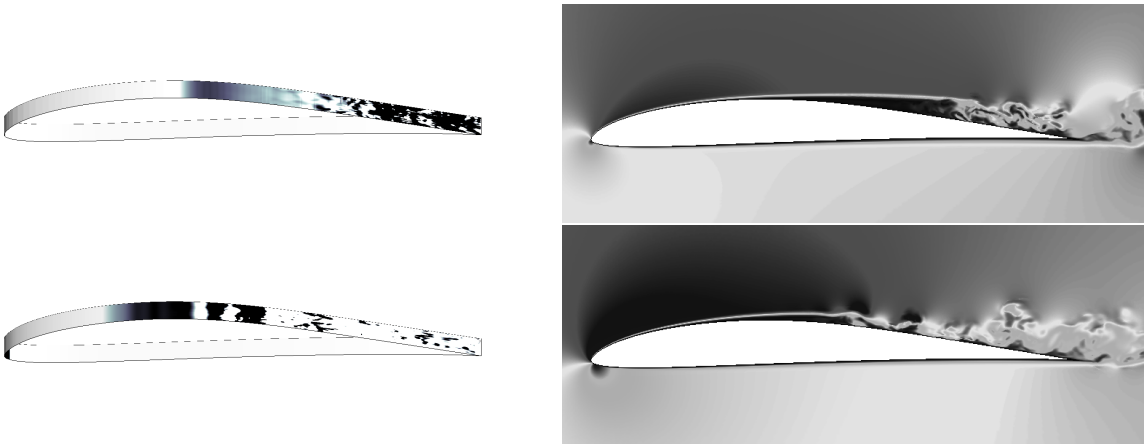

Figure 3. E387 LES separation: instantaneous x-aligned negative component of the friction (left, from black, fully detached to white, attached flow) and instantaneous velocity norm $\|u\|$ in one plane (right, dark corresponds to high values) at $\alpha = 4^\circ$ (top) and $\alpha = 8^\circ$ (bottom).

To determine the LSB and reattachment locations precisely, averaged chordwise pressure and skin friction distributions are presented on Figures 4 and 5. The LES results have been averaged over three flow passage times as well as along the span. At $\alpha = 4^\circ$, the two different flow configurations observed in the experiment are presented with a lower performance at $TI = 0.20\%$ than at $TI = 0.16\%$. The URANS results are close to the lower performance case ($TI = 0.20\%$) and this even when changing the N_{crit} of the transition model. The LES results are very well matching the higher performance case as expected as it is the case with the lower TI. XFOIL

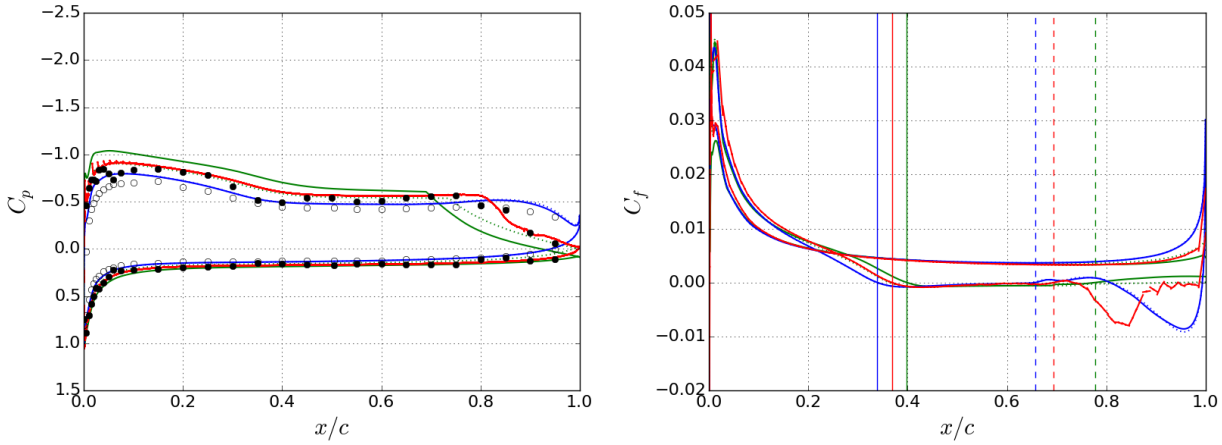

Figure 4. Comparison of the chordwise pressure coefficient (left) and friction coefficient (right) obtained at $\alpha = 4°$ and $Re = 6 \times 10^4$ with XFOIL (solid $N_{crit} = 7$ and dotted $N_{crit} = 9$ green curves), URANS (solid $N_{crit} = 7$ and dotted $N_{crit} = 9$ blue curves) and LES (red curves) to the experimental results (black $TI = 0.16\%$ and white $TI = 0.20\%$ circles) from [24]. Vertical solid and dashed lines present respectively the separation and reattachment locations.

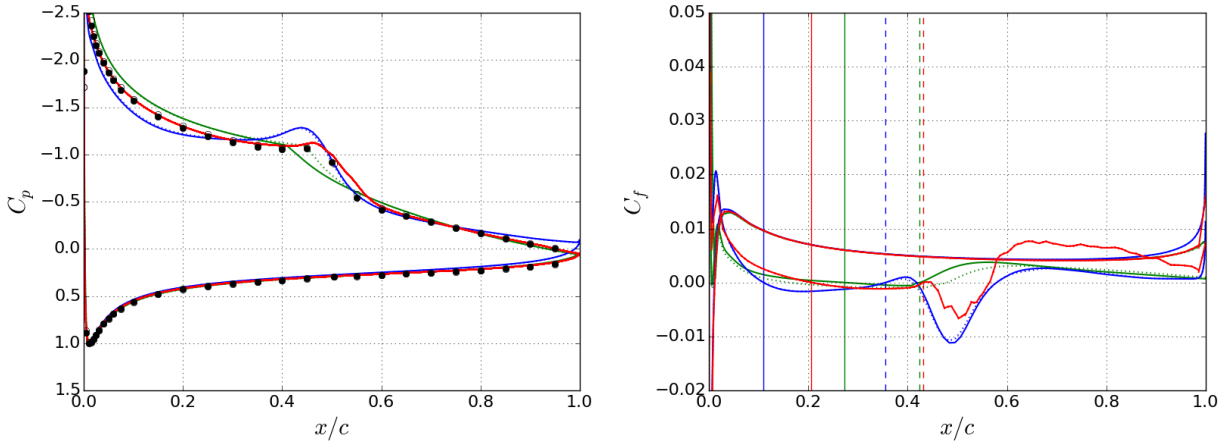

Figure 5. Comparison of the chordwise pressure coefficient (left) and friction coefficient (right) obtained at $\alpha = 8°$ and $Re = 6 \times 10^4$ with XFOIL (solid $N_{crit} = 7$ and dotted $N_{crit} = 9$ green curves), URANS (solid $N_{crit} = 7$ and dotted $N_{crit} = 9$ blue curves) and LES (red curves) to the experimental results (black $TI = 0.16\%$ and white $TI = 0.20\%$ circles) from [24]. Vertical solid and dashed lines present respectively the separation and reattachment locations.

results are overestimating the performance, even compared to the experiment with the highest performance ($TI = 0.16\%$). Contrarily to the URANS results, an effect of the N_{crit} parameter is observed on the XFOIL results with an increase in performance for reduced TI, as observed experimentally. At $\alpha = 8°$, no turbulence effect is observed anymore and the LES results are the closest to the experiment.

On the pressure curve the laminar part of the LSB is identified by the pressure plateau. The sign changes of the skin friction are used to locate the flow separation and reattachment points listed in Table 1. The experimental data, obtained at a slightly higher Reynolds number, are also given for comparison as there were almost no Reynolds number effect observed experimentally

	Re	TI	$\alpha = 4°$		$\alpha = 8°$	
			Separation	Reattachment	Separation	Reattachment
XFOIL	6×10^4	0.16%	0.40	0.78	0.27	0.42
		0.07%	0.36	0.95	0.16	0.48
URANS	6×10^4	$0.07\% - 0.16\%$	0.34	0.66	0.11	0.36
LES	6×10^4	0.00%	0.37	0.69	0.21	0.43
exp.	1×10^5	0.16%	0.35	0.73	0.29	0.47

Table 1. Comparison of the computational and experimental separation and reattachment locations at $\alpha = 4$ and $8°$ for different inflow turbulence intensities.

regarding separation and reattachment locations [24].

From these results, it seems that the difference between the computational results could be due to a better capture of the LSB by LES. However, due to the high sensitivity of the experiments and reference models to the TI, no strong conclusion should be taken regarding the small mismatch on the pressure distribution of the state-of-the-art tools. This evaluation on a low Reynolds number airfoil is however very positive for the DG methodology .

4. WMLES of high Reynolds number airfoil

The NACA4412 airfoil has been chosen as it is a well documented test case frequently used in code comparisons and as it has been recently used for testing WMLES approaches [25, 26]. Even if the main benchmark on this airfoil (NASA 2DN44 benchmark) is at $Re = 1.52 \times 10^6$ and $\alpha = 13.87°$, based on the Coles and Wadcock experiment from 1979 [27], the current simulations are using a later experiment performed by Wadcock in 1987 [28], which is considered as less impacted by the strong tunnel effects observed in the 1979 experiment. This experiment provides results at $Re = 1.64 \times 10^6$ and $\alpha = 12.0°$.

At this condition, the flow presents a small laminar region, a laminar/turbulent transition and separates close to the trailing-edge, at $\simeq 85\%$ of the chord [28]. As the wall model used here is based on the Reichardt law which assumes a turbulent flow in equilibrium, the laminar region, the transition and the separation will a priori not be captured adequately by the model. It is interesting however to evaluate the performance of the cheapest computational model before testing more complex models.

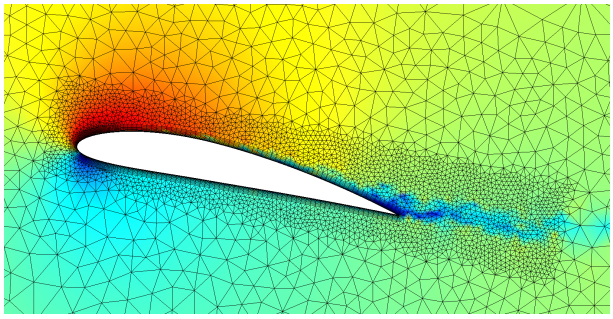

Figure 6. Instantaneous velocity field obtained at $\alpha = 12°$ and $Re = 1.64 \times 10^6$ with WMLES.

Figure 6 presents an instantaneous velocity field in one plane together with the mesh for the WMLES computation. The mesh methodology is equivalent to the one used for the E387 but whereas the RANS mesh has been refined to keep $y^+ \simeq 2$, the WMLES mesh has been kept almost identical to the one at $Re = 6 \times 10^4$, leading to 8.4M dof with $\Delta y^+ \simeq 100$, Δx^+ and $\Delta z^+ \simeq 200$ and third order accurate resolution ($p = 2$) in the wall-adjacent cell and fourth

order accurate resolution ($p = 3$) in the rest of the domain as suggested by previous WMLES experience [29]. This mesh is too coarse to represent the inner layer and needs a wall model. According to the requirements detailed in a recent review on WMLES [30], this mesh is even too coarse for correctly resolving the outer layer and performing WMLES at some locations. This is due to the fact that the boundary layer grows by a factor of 1000 along the chord, leading to too coarse mesh close to the leading-edge (laminar region) and too fine mesh close to the trailing-edge compared to the WMLES guidelines. The result obtained with this mesh and basic model have thus to be considered as a first step in understanding wall model potential for performing high Reynolds number LES of airfoil flows.

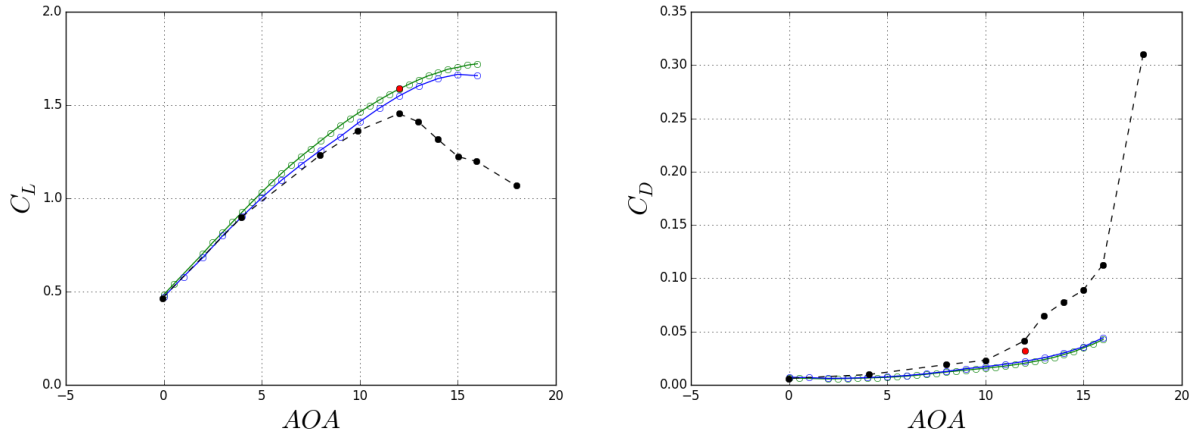

Figure 7. NACA4412: comparison of computational lift and drag (XFOIL: green, RANS: blue and WMLES: red circle) to Wadcock [28] experiment (black circles).

As for the E387, the WMLES results presented here have been averaged in span and in time over three flow passage times. Figure 7 compares the lift and drag coefficients obtained numerically to the experiment by Wadcock [28]. As the panel and RANS computations, also the WMLES results overestimate the lift. The three modeling tools provide similar lift and WMLES provide a slightly better prediction of the drag. To be able to quantify the quality of this result, LES with the same mesh but with no-slip wall conditions on the airfoil surface, hence coarse LES, have been performed. The case with no-slip condition did not converge, likely due to the too coarse mesh, not able to capture the gradients. This shows that, although not perfect, the wall model indeed helps in improving the lift and drag estimate.

Figure 8 provides the chordwise pressure distribution obtained with XFOIL, RANS and WMLES compared to the experimental results. The main behavior is captured by XFOIL, RANS and WMLES but they underestimate the suction in the last 20% of the chord; this is likely due to the fact that they do not capture the trailing-edge separation observed in the experiment. To evaluate the capture of the trailing-edge separation, Figure 8 provides as well the chordwise friction distribution obtained with XFOIL, RANS and WMLES. It appears that XFOIL and RANS predict well the separation location observed by Wadcock [28] at 85% but not WMLES, for which the flow stays fully attached.

To compare the way the codes predict separation, Figure 9 compares the obtained experimental and computational velocity profiles. The extensive database from Wadcock [28] contains the velocity and fluctuations profiles in the three directions on three locations on the airfoil suction side and two locations in the wake. In this paper, as a first evaluation, only the main average velocity component will be compared. For the three locations on the airfoil, this is the tangential velocity, whereas for the two wake cases, it is the velocity parallel to the wind

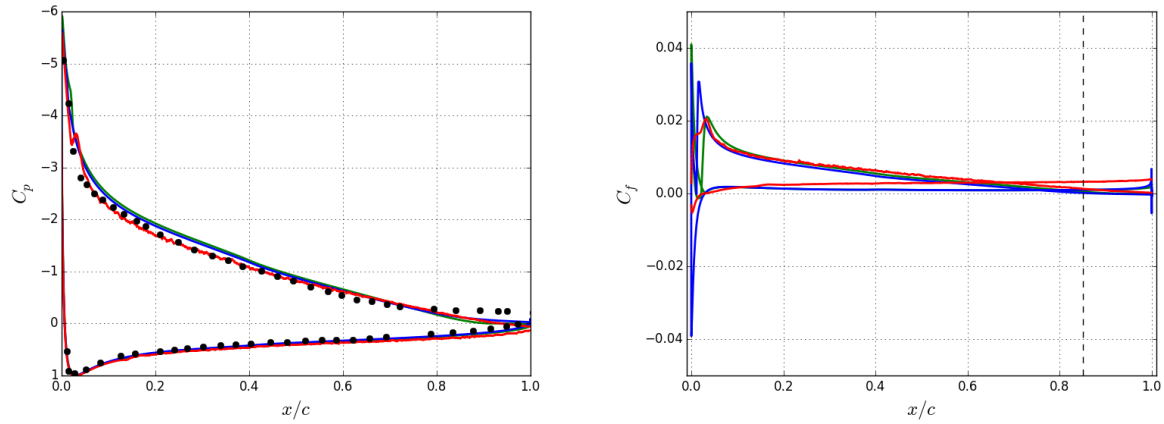

Figure 8. NACA4412: comparison of the chordwise pressure coefficient (left) and friction coefficient (right) obtained at $\alpha = 12°$ and $Re = 1.64 \times 10^6$ with XFOIL (green), RANS (blue) and WMLES (red) to the experimental results (black circles) from Wadcock [28]. The vertical black dashed line represents the separation observed in the experiment [28].

tunnel wall surface as presented on Figure 9.

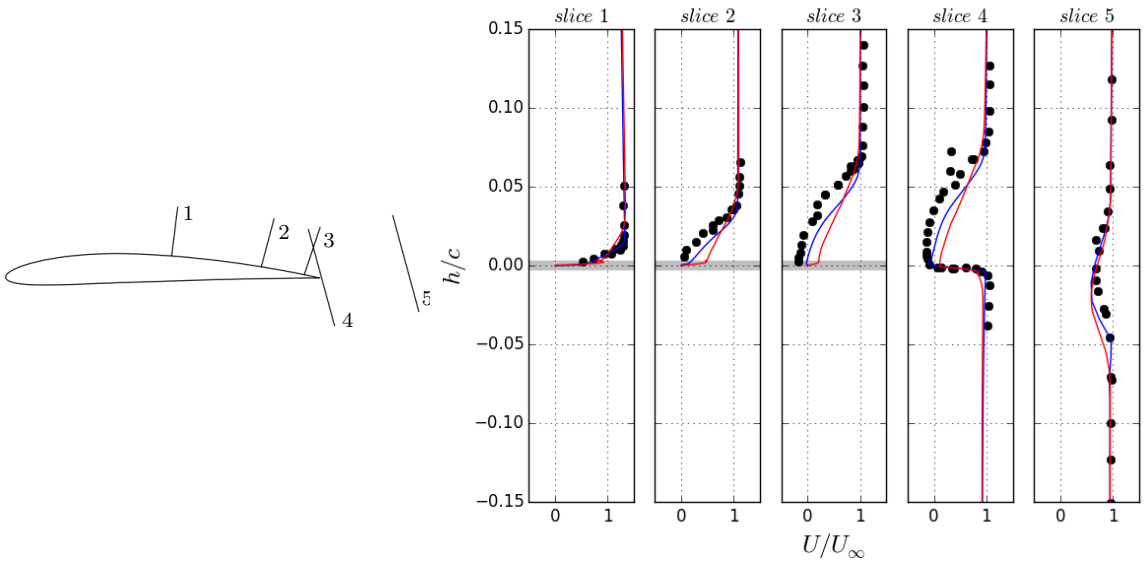

Figure 9. Left: schematic of the measurement slices with from left to right, slices perpendicular to the airfoil suction surface at $x/c = 0.529, 0.815, 0.952$ and to the wind tunnel bottom wall at $x_t/c = 0.007, 0.282$. Right: comparison of the mean tangential velocity profiles obtained on these slices with RANS (blue), WMLES (red) and Wadcock [28] experiment (black circles).

It would seem from this comparison that RANS is better capturing the trailing-edge separation than WMLES, which slightly underestimates the deceleration of the flow due to the adverse pressure gradient. This was however expected as the wall model used here does not take the pressure gradient into account. Therefore it is believed that the use of a more elaborate wall model would significantly improve the results.

5. Conclusions and perspectives

Although the DG methodology has shown high accuracy and scalability, it is not used yet in the wind energy sector. In this study, the DG methodology is used to characterize airfoil aerodynamics. At low Reynolds number ($Re = 6 \times 10^4$), LES of the Eppler 387 airfoil at $\alpha = 4^o$ and $\alpha = 8^o$ are in very good agreement with the experiment, slightly better capturing the pressure distribution than the state-of-the-art tools (RANS and XFOIL). At high Reynolds number ($Re = 1.64 \times 10^6$), the WMLES approach is tested on the NACA4412 airfoil. At this high Reynolds number, the three methods provide equivalent results. In view of the high computational difference between the methods (few seconds (XFOIL), $\approx$ 10 minutes on 10 CPU ((U)RANS), $\approx$ 2 days on 500 CPU (WMLES)), the WMLES approach presented here has no added-value yet compared to the state-of-the-art tools. But, although the wall stress model is so far very basic, i.e. not supposed to handle separation nor adverse pressure gradient, the present WMLES already provides quite acceptable results. The present study hence constitutes a confidence-inspiring step in our effort towards the use of LES at high Reynolds number.

It is expected that more advanced wall model will be required to improve the results. The Two-Layer Model [11] has provided good results on multiple test cases including a backward facing step [31], a trailing-edge [32] and an airfoil near stall [33]. Adding this approach to the presented WMLES would likely permit to improve strongly the results. This feature is currently being implemented and tested.

Acknowledgments

The first author gratefully acknowledges Corentin Carton de Wiart (NASA Ames Research Center) for his contribution to the WMLES implementation in Argo and Torben J. Larsen (DTU Wind) for his support through the APPLES PhD project.

This research has been financed by the IRP Wind Mobility scheme and by the Walloon Region through the FirstDoCA framework. The present research benefited from computational resources made available on the Tier-1 supercomputer of the Fédération Wallonie-Bruxelles which is infrastructure funded by the Walloon Region under the grant agreement $n°1117545$.

References

[1] Carton de Wiart C, Hillewaert K, Duponcheel M and Winckelmans G 2013 *Int. J. Numer. Meth. Fluids* **74** 469–493 doi: 10.1002/fld.3859
[2] Hillewaert K 2013 *Development of the Discontinuous Galerkin Method for high-resolution, large scale CFD and acoustics in industrial geometries* Ph.D. thesis Ecole polytechnique de Louvain/iMMC
[3] Frère A, Hillewaert K, Sarlak H, Mikkelsen R F and Chatelain P 2015 *Proc. 33rd ASME Wind* (Kissimmee: American Institute of Aeronautics & Astronautics)
[4] Carton de Wiart C 2014 *Towards a discontinuous Galerkin solver for scale-resolving simulations of moderate Reynolds number flows, and application to industrial cases* Ph.D. thesis Ecole polytechnique de Louvain/iMMC
[5] Carton de Wiart C, Hillewaert K, Bricteux L and Winckelmans G *Proceedings of the ERCOFTAC Workshop "Direct and Large-Eddy Simulation 9"* (Dresden, Germany: ERCOFTAC)
[6] Carton de Wiart C and Hillewaert K 2012 *Seventh International Conference on Computational Fluid Dynamics* (Hawai, USA)
[7] Hillewaert K, Carton de Wiart C, Verheylewegen G and Arts T 2014 *Proceedings of the ASME Turbine Technical Conference and Exhibition* GT2014-26739 (ASME Turbo Expo 2014)
[8] Choi H and Moin P 2012 *Physics of fluids* **24**
[9] Piomelli U and Balaras E 2002 *Annual Review of Fluid Mechanics*
[10] Spalart P, Jou W, Strelets M and Allmaras S 1997 *Advances in DNS/LES* (Columbus, OH: Greyden) pp 137–148
[11] Balaras E, Benocci C and Piomelli U 1996 *AIAA journal* **34** 1111–1119
[12] Lee M and Moser R D 2015 *Journal of Fluid Mechanics* **774** 395–415
[13] Michelsen J 1992 Basis3D - a Platform for Development of Multiblock PDE Solvers Technical Report AFM 92-05, Technical University of Denmark, Department of Fluid Mechanics, Technical University of Denmark

[14] Michelsen J 1994 Block structured Multigrid solution of 2D and 3D elliptic PDE's Technical Report AFM 94-06, Technical University of Denmark, Department of Fluid Mechanics, Technical University of Denmark
[15] Sørensen N 1995 General Purpose Flow Solver Applied to Flow over Hills Risø-R- 827-(EN), Risø National Laboratory, Roskilde, Denmark
[16] Leonard B P 1979 *Computer methods in applied mechanics and engineering* **19** 59–98
[17] Menter F 1993 Zonal Two Equation k-ω Turbulence Models for Aerodynamic Flows *AIAA paper 1993-2906*
[18] Michelsen J 2002 *Forskning i aeroelasticitet EFP-2001*, chapter beregning af laminar-turbulent omslag i 2d og 3d, page 73 Risø-R1349(DA) in Danish
[19] Sørensen N 1998 HypGrid2D a 2-D Mesh Generator Risø-R- 1035-(EN), Risø National Laboratory, Roskilde, Denmark
[20] McGhee R J, Walker B S and Millard B F 1988 Experimental results for the Eppler 387 airfoil at low Reynolds numbers in the Langley low-turbulence pressure tunnel Tech. Rep. TM-4062 NASA Langley Research Center, Hampton, Virginia
[21] Volker D 1977 Preliminary results of windtunnel measurements on some airfoil sections at Reynolds numbers between 0.6×10^5 and 5.0×10^5 Memo. M-276 Delft Univ. of Technology
[22] Selig M S, Donovan J F and Fraser D B 1989 Airfoils at Low Speeds H.A. Stokely publisher, Virginia, USA
[23] Althaus D 1980 Profilpolaren für den Modellflug: Windkanalmessungen an Profilen im Kritischen Reynoldszahlbereich Neckar-Verlag Villingen-Schwenningen, Germany
[24] McGhee R J, Walker B S and Millard B F 1988 Tech. Rep. TM-4062 (Hampton: NASA)
[25] Park G I and Moin P 2014 *Physics of Fluids (1994-present)* **26** 015108
[26] Bose S and Moin P 2014 *Physics of Fluids (1994-present)* **26** 015104
[27] Coles D and Wadcock A J 1979 *AIAA Journal* **17** 321–329
[28] Wadcock A J 1987 Investigation of low-speed turbulent separated flow around airfoils Nasa - 177450 NASA Ames Research Center
[29] Frère A, Carton de Wiart C, Hillewaert K, Chatelain P and Winckelmans G Applying wall models in discontinuous Galerkin implicit LES in preparation for IJNMF
[30] Larsson J, Kawai S, Bodart J and Bermejo-Moreno I 2016 *Mechanical Engineering Reviews* **3** 15–00418–15–00418
[31] Cabot W and Moin P 2000 *Flow, Turbulence and Combustion* **63** 269–291
[32] Wang M and Moin P 2002 *Physics of Fluids* **14** 2043–2051
[33] Kawai S and Asada K 2013 *Computers & Fluids* **85** 105 – 113